cells treated with scrambled siRNA (Fig. 3C). Furthermore, this reduced ability to induce *hsp70i* protein was correlated with a significant increase in cell death after stress treatment (Fig. 3D), which indicates the critical importance of HSF2-mediated *hsp70i* bookmarking for cell stress survival.

The results above show that in mitotic cells, HSF2 binds the *hsp70i* promoter, interacts with the CAP-G subunit of condensin, and is critical for the bookmarking of this promoter. But how does HSF2 mediate inhibition of condensin activity at this locus? Condensin activity requires phosphorylation of the CAP-G, CAP-D2, and CAP-H subunits by the mitotic kinase Cdc2–cyclin B (*21*, *22*). We previously showed that HSF2 interacts with the serine-threonine protein phosphatase 2A (PP2A) (*23*), and other studies have suggested that a member of the PPP family of serine-threonine phosphatases, which includes PP2A, is involved in dephosphorylating the condensin subunits that are phosphorylated by Cdc2 (*24*). On the basis of these data, we hypothesized that HSF2 mediates *hsp70i* promoter bookmarking by recruiting PP2A to this promoter. When condensin interacts with HSF2 via CAP-G, it could be dephosphorylated and inactivated by the HSF2-associated PP2A to prevent compaction of this region of DNA. Supporting this hypothesis, immunoprecipitation experiments demonstrate that HSF2 does associate with PP2A in mitotic cells, and that more of the complex is observed in mitotic than in asynchronous cells, suggesting mitosis-dependent regulation of this interaction (Fig. 4A). Furthermore, ChIP assays show that PP2A exists within cross-linking distances of the *hsp70i* promoter in mitotic cells and that more association is observed in mitotic cells than in asynchronous cells (Fig. 4B). To confirm the function of PP2A as a condensin phosphatase, we isolated condensin by immunoprecipitation with CAP-G antibodies, phosphorylated it with purified Cdc2–cyclin B and [γ-^{32}P]adenosine triphosphate (ATP) in vitro, and then incubated the phosphorylated condensin with purified PP2A. The results show that PP2A can dephosphorylate CAP-G, CAP-D2, and CAP-H (fig. S3A). Finally, we took advantage of the ability of the Mpm2 antibody to detect the phosphorylated forms of Cdc2–cyclin B substrates, including CAP-G (*25*), to show that HSF2 immunoprecipitates from mitotic cells contain an okadaic acid–inhibitable phosphatase activity that can efficiently dephosphorylate phosphorylated CAP-G that was immunoprecipitated from mitotic cells (Fig. 4C). This activity is not detected in HSF1 immunoprecipitates from mitotic cells (fig. S3B).

The results in this paper suggest that HSF2 mediates *hsp70i* promoter bookmarking by binding to this promoter in mitotic cells, recruiting PP2A, and interacting with condensin enzyme by binding to the CAP-G subunit to allow the PP2A to dephosphorylate efficiently and to inactivate this condensin, thereby preventing compaction of this region of chromosomal DNA. The results also demonstrate the biological importance of bookmarking by showing that the loss of HSF2-mediated bookmarking significantly reduces the ability of cells to induce *hsp70i* gene expression and to survive stress. This knowledge opens the door to investigating the mechanisms and biological roles of other gene bookmarking events, toward understanding the full biological ramifications of bookmarking for cell function.

References and Notes

1. T. Hirano, *Cell Cycle* **3**, 26 (2004).
2. A. V. Strunnikov, *Prog. Cell Cycle Res.* **5**, 361 (2003).
3. K. A. Hagstrom, B. J. Meyer, *Nature Rev. Genet.* **4**, 520 (2003).
4. J. R. Swedlow, T. Hirano, *Mol. Cell* **11**, 557 (2003).
5. K. Yokomori, *Curr. Top. Microbiol. Immunol.* **274**, 79 (2003).
6. E. F. Michelotti, S. Sanford, D. Levens, *Nature* **388**, 895 (1997).
7. R. Christova, T. Oelgeschlager, *Nature Cell Biol.* **4**, 79 (2002).
8. S. John, J. L. Workman, *Bioessays* **20**, 275 (1998).
9. M. A. Martinez-Balbas, A. Dey, S. K. Rabindran, K. Ozato, C. Wu, *Cell* **83**, 29 (1995).
10. E. S. Christians, L. J. Yan, I. J. Benjamin, *Crit. Care Med.* **30**, S43 (2002).
11. L. Pirkkala, P. Nykanen, L. Sistonen, *FASEB J.* **15**, 1118 (2001).
12. C. Jolly, R. I. Morimoto, *J. Natl. Cancer Inst.* **92**, 1564 (2000).
13. K. A. Morano, D. J. Thiele, *Gene Expr.* **7**, 271 (1999).
14. T. J. Schuetz, G. J. Gallo, L. Sheldon, P. Tempst, R. E. Kingston, *Proc. Natl. Acad. Sci. U.S.A.* **88**, 6911 (1991).
15. K. D. Sarge, V. Zimarino, K. Holm, C. Wu, R. I. Morimoto, *Genes Dev.* **5**, 1902 (1991).
16. M. L. Goodson *et al.*, *J. Biol. Chem.* **276**, 18513 (2001).
17. F. L. Sun *et al.*, *Proc. Natl. Acad. Sci. U.S.A.* **97**, 5340 (2000).
18. T. H. Li, C. Kim, C. M. Rubin, C. W. Schmid, *Nucleic Acids Res.* **28**, 3031 (2000).
19. B. J. Deroo, T. K. Archer, *Mol. Biol. Cell* **12**, 3365 (2001).
20. T. Wang, W. P. Lafuse, K. Takeda, S. Akira, B. S. Zwilling, *J. Immunol.* **169**, 795 (2002).
21. K. Kimura, M. Hirano, R. Kobayashi, T. Hirano, *Science* **282**, 487 (1998).
22. K. Kimura, O. Cuvier, T. Hirano, *J. Biol. Chem.* **276**, 5417 (2001).
23. Y. Hong, K. D. Sarge, *J. Biol. Chem.* **274**, 12967 (1999).
24. T. Hirano, R. Kobayashi, M. Hirano, *Cell* **89**, 511 (1997).
25. A. Takemoto, K. Kimura, S. Yokoyama, F. Hanaoka, *J. Biol. Chem.* **279**, 4551 (2004).

26. We are grateful to K. Yokomori and M. Matunis for generously providing antibodies and to R. Hilgarth and L. Murphy for insightful discussions. This research was supported by NIH grants GM61053, GM64606 (K.D.S.), and HD36879, HD41609 (O.-K.P.-S.).

Supporting Online Material

www.sciencemag.org/cgi/content/full/307/5708/421/DC1
Materials and Methods
Figs. S1 to S3
References and Notes

18 October 2004; accepted 24 November 2004
10.1126/science.1106478

Mathematical Modeling of Planar Cell Polarity to Understand Domineering Nonautonomy

Keith Amonlirdviman,[1] Narmada A. Khare,[2] David R. P. Tree,[2] Wei-Shen Chen,[2] Jeffrey D. Axelrod,[2]*† Claire J. Tomlin[1]*†

Planar cell polarity (PCP) signaling generates subcellular asymmetry along an axis orthogonal to the epithelial apical-basal axis. Through a poorly understood mechanism, cell clones that have mutations in some PCP signaling components, including some, but not all, alleles of the receptor *frizzled*, cause polarity disruptions of neighboring wild-type cells, a phenomenon referred to as domineering nonautonomy. Here, a contact-dependent signaling hypothesis, derived from experimental results, is shown by reaction-diffusion, partial differential equation modeling and simulation to fully reproduce PCP phenotypes, including domineering nonautonomy, in the *Drosophila* wing. The sufficiency of this model and the experimental validation of model predictions reveal how specific protein-protein interactions produce autonomy or domineering nonautonomy.

As the understanding of cellular regulatory networks grows, system behaviors resulting from feedback effects have proven sufficiently complex so as to preclude intuitive understanding. The challenge now is to show that enough of a network is understood to explain such behaviors. Using mathematical modeling, we show the sufficiency of a proposed biological model and study its properties, to demonstrate that it can explain complex PCP phenotypes and to provide insight into the system dynamics that govern them.

Many epithelia are polarized along an axis orthogonal to the apical-basal axis. On the *Drosophila* adult cuticle, each hexagonally packed cell elaborates an actin-rich hair that develops from the distal vertex and points distally (Fig. 1A). Genetic analyses have identified a group of PCP proteins whose activities are required to correctly polarize

these arrays (*1*, *2*). The domineering nonautonomy adjacent to cell clones mutant for some, but not other, PCP genes has not yet been adequately explained (*1*). For example, in the *Drosophila* wing, *Van Gogh/strabismus* (*Vang*; encoding a four-pass transmembrane protein) (*3*, *4*) clones disrupt polarity proximal to the mutant tissue (*3*), whereas null *frizzled* (*fz*; encoding a seven-pass transmembrane protein) alleles disrupt polarity distal to the clone (*5*, *6*). Models to explain this phenomenon have often invoked diffusible factors, referred to as factor X or Z, because they have not yet been identified (*1*, *7*–*15*). We propose instead that the observed behaviors of known PCP proteins are sufficient to explain domineering nonautonomy.

Fz and other PCP signaling components accumulate selectively on the distal or proximal side of wing cells (Fig. 1A). Evidence has been provided that these proteins function in a feedback loop that amplifies an asymmetry cue, which converts uniform distributions of PCP proteins into highly polarized distributions (*11*, *16*–*18*) (Fig. 1B). The proposed feedback mechanism depends on several functional relationships (*18*). Fz recruits Dishevelled (Dsh; a cytoplasmic protein) to the cell membrane (*16*, *19*). In addition, Fz promotes the recruitment of Prickle-spinylegs (Pk; a LIM domain protein) (*5*, *18*, *20*) and Vang (*21*) to the cell membrane of the adjacent cell. Feedback is provided by the ability of Pk [and Vang; supporting online material (SOM)] to cell-autonomously block Fz-dependent recruitment of Dsh (*18*). This feedback loop functions strictly locally, between adjacent cells. Global directionality is imposed through the agency of the novel transmembrane protein Four-jointed and the cadherins Dachsous and Fat (Ft) (*22*–*24*). Widerborst, a regulatory subunit of protein phosphatase 2A, accumulates asymmetrically within each cell and is required to bias the feedback loop (*25*). Although the mechanism by which Ft biases the direction of the feedback loop is unknown, one possibility is that Ft may direct Widerborst distribution.

However, it is not readily apparent that this biological model does not readily explain the complex patterns observed in fields of cells containing mutant clones, and others have argued that it cannot account for some of the observed phenotypes (*1*, *26*). Indeed, progress in understanding PCP signaling has been hampered by an inability to deduce, given a particular signaling network hypothesis, definitive links between molecular genetic interventions and tissue patterning effects. For example, although it is apparent that removing Dsh or Fz would disrupt the feedback loop, it is not obvious how the feedback loop in adjacent wild-type cells responds, such that *dsh* mutant clones behave autonomously, whereas for most *fz* alleles, mutant clones behave nonautonomously. Interestingly, though, for some *fz* alleles, mutant clones produce an almost cell-autonomous phenotype (*5*, *6*, *27*). As another example, Pk overexpression promotes the asymmetric accumulation of Dsh and Fz (*18*), despite the role of Pk in the feedback loop as an inhibitor of Dsh membrane recruitment.

We have developed a mathematical model based on the described feedback loop and an initial asymmetry input representing the global directional cue (*18*, *22*, *23*). Although mathematical modeling cannot prove the correctness of the underlying biological model, the ability of the mathematical model to capture the known behaviors of the system proves the feasibility of the biological model, provides testable

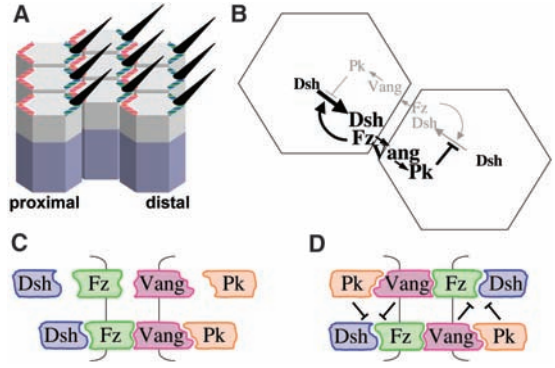

Fig. 1. Illustrations of PCP. (**A**) Hexagonally packed wing cells accumulate Fz and Dsh distally (blue/green) and Pk and Vang proximally (pink/orange). A hair is elaborated from the distal vertex of each cell. (**B**) A local feedback loop model for a PCP signaling mechanism. Black lettering indicates protein accumulation. Gray lettering indicates proteins whose concentrations are decreased. (**C**) Representation of proposed binding interactions. (**D**) Inhibition model representing disruption of the Dsh-Fz interaction by Pk and Vang.

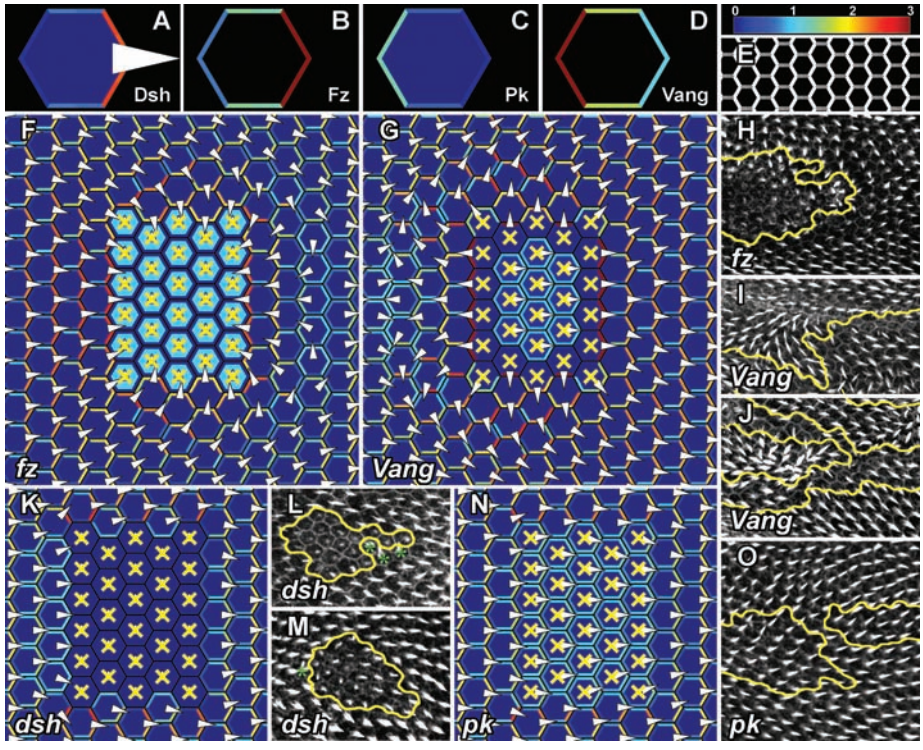

Fig. 2. Simulation results. Wild-type results showing the final distributions of Dsh (**A**), Fz (**B**), Pk (**C**), and Vang (**D**). The same color scale is used in all figures, where 1 is scaled to the initial uniform concentration of Dsh and the scale is truncated so that concentrations greater than 3 are shown in red. (**E**) Simulated distribution of Dsh displayed as an intensity representing total Dsh concentrations, corresponding to the appearance of Dsh::GFP in wild-type experiments. Simulation results of several PCP phenotypes showing the final distribution of Dsh with predicted hair growth directions derived from the vector sum of Dsh (**F**, **G**, **K**, and **N**) and corresponding pupal wings (**H** to **J**, **L**, **M**, and **O**). Greater Dsh asymmetry is represented by hair placement at increasing distances from the cell center. When Dsh asymmetry does not exceed the threshold value, the hair is depicted at the center of the cell. Mutant cells are designated with yellow. (H) fz^{R52} null clones. (**I**) and (J) $Vang^{A3}$ mutant clones. (L and M) dsh^{V26} mutant clones. (O) *pk-sple*^{13} mutant clones. Asterisks mark nonautonomous effects near *dsh* clones.

[1]Department of Aeronautics and Astronautics, Stanford University, Stanford, CA 94305–4035, USA. [2]Department of Pathology, Stanford University School of Medicine, Stanford, CA 94305–5324, USA.

*These authors contributed equally to this work.
†To whom correspondence should be addressed. E-mail: tomlin@stanford.edu (C.J.T.); jaxelrod@stanford.edu (J.D.A.)

hypotheses, and yields insight into the factors contributing to autonomy and nonautonomy.

We have represented the features of the biological feedback loop model as a mathematical reaction-diffusion model (*28*) that describes the concentrations of Dsh, Fz, Vang, and Pk throughout a network of cells. Although the mechanisms that underlie the local feedback loop are not fully understood, the essential logic of this feedback loop is preserved by representing these interactions as binding to form protein complexes (Fig. 1, C and D).

Inhibition of Dsh membrane recruitment by Pk and Vang (Fig. 1, C and D, SOM) is represented in the mathematical model as an increase in the backward reaction rate of reactions in which Dsh binds Fz (or Fz complexes) by a factor dependent on the local concentration of Pk and Vang. The specific mechanism for the introduction of the directional bias into the feedback loop network is not known. Two forms of a global biasing signal were therefore implemented, and the results using either of these models were similar (SOM). The resulting mathematical model consists of a system of 10 nonlinear partial differential equations. With a given set of model parameters, an array of cells could then be simulated, and the resulting hair pattern assigned on the basis of the final distribution of Dsh.

The model parameters, including the initial protein concentrations, reaction rates, and diffusion constants, were not known, and so these parameters were identified by constraining them to result in specific qualitative features of the hair pattern phenotypes. A sensitivity analysis showed that the model results are not highly sensitive to the precise parameter values and suggests that our conclusions regarding the feasibility of the model are valid for considerable ranges of parameters. The full development and discussion of assumptions for the mathematical model are in the SOM text.

In simulated wild-type cells (Fig. 2, A to E), Dsh and Fz localize to the distal membrane, and Vang and Pk localize to the proximal membrane, as is seen in vivo (*16*–*18*, *21*). Simulated clones of cells lacking *fz* function disrupt polarity in wild-type cells distal to the clones [Fig. 2F, compare with 2H (*5*, *6*)], whereas simulated clones lacking *Vang* function disrupt polarity on the proximal side of the clones [Fig. 2G, compare with 2, I and J; (*3*)]. Simulated clones lacking *dsh* function result in the disruption of polarity within the mutant cells, but only show a mild effect outside of the clones (Fig. 2K). The nearly, though not fully cell autonomous, phenotype is similar to that which we observed experimentally [Fig. 2, L and M; and (*29*)]. Clones lacking all *pk* function show only a subtle phenotype [Fig. 2, N and O; (*20*)]. Examination of protein distributions (Fig. 2; fig. S7) shows that the results are highly concordant with published observations (table S2). Similarly, simulated overexpression clones produce results closely mimicking observed experimental results (fig. S8). In simulations and in wings, relatively small clones lacking a global biasing signal show no phenotype, demonstrating that not all cells need to respond to the global directional signal for the feedback loop to cooperatively align all of the cells (*23*, *30*).

Previously, we found that Pk overexpression in the posterior wing domain enhanced the accumulation of Fz and Dsh at cell boundaries, despite the observed ability of Pk and Vang to block Dsh recruitment (*18*). Consistent with these results, Dsh and Fz are seen in a simulation of this experiment to accumulate to higher levels in the region overexpressing *pk* than in the wild-type region, and they accumulate perpendicular to the wild-type orientation near the anterior-posterior boundary (Fig. 3).

Our results suggested a mechanistic explanation for the difference between autonomous and nonautonomous *fz* alleles. Because the nearly autonomous *fz* alleles [fz^{J22} and fz^{F31}; (*27*)] have phenotypes similar to *dsh* clones, we hypothesized that these alleles may be selectively deficient in complexing with Dsh, but normal in their ability to complex with Vang (Fig. 4A). Simulations of clones in which we disrupted the interaction between Dsh and Fz by reducing the corresponding forward reaction rates produced nearly cell autonomous polarity phenotypes (Fig. 4B and fig. S9).

This hypothesis makes two easily testable predictions. First, Fz autonomous proteins should be present in the membrane and should recruit Vang to the adjacent membrane, whereas Fz nonautonomous protein should not recruit Vang. It has previously been shown that GFP-tagged Fz^{J22}, expressed in a wild-type background, is present at the apical cell cortex, but remains symmetrically distributed (*17*), a distribution in accordance with our simulation of this condition (fig. S11). Examining this further, we found that in cells adjoining clones of the autonomous fz^{F31} al-

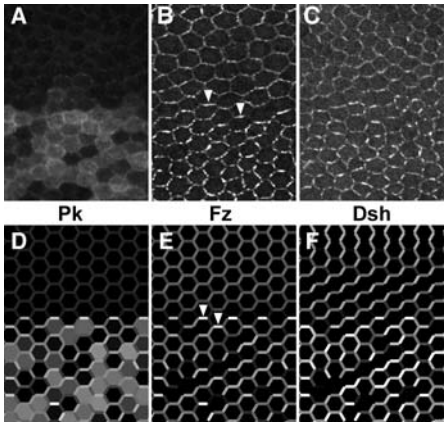

Fig. 3. *pk* overexpression. Pk (**A**), Fz::GFP (**B**) and Dsh::GFP (**C**) near the anterior-posterior boundary of pupal wings overexpressing *pk* in the *engrailed* domain. (**D** to **F**) Simulation of a periodic horizontal band of random 1*x* – 11.58*x* *pk* overexpression, showing Pk (D), Fz (E) and Dsh (F). Reorientation of Fz accumulation is denoted with arrowheads. (A to C) are different wings.

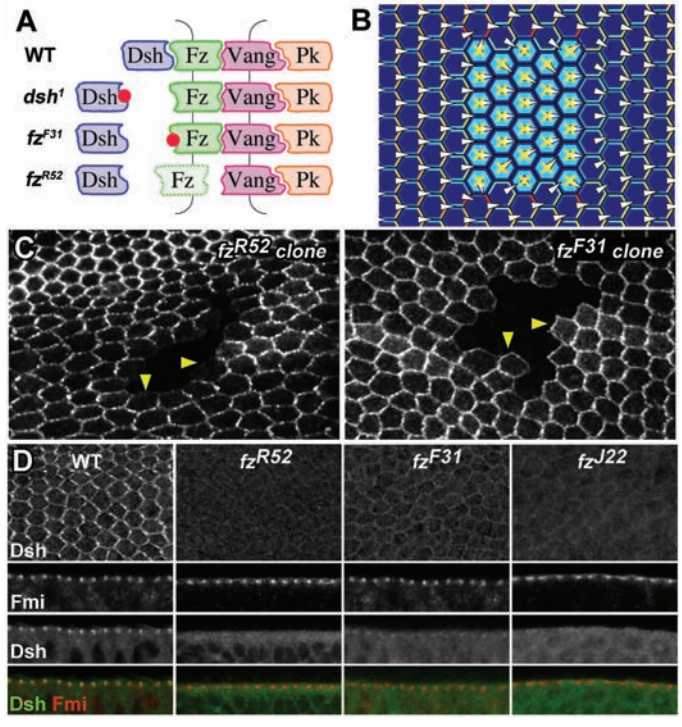

Fig. 4. Cell autonomy. (**A**) Interactions for wild-type, Dsh^1, Fz autonomous, and Fz nonautonomous alleles. Red dots indicate point mutations, and the faded Fz indicates absent protein in some null alleles. Spaces between proteins indicate loss of interaction. (**B**) Simulation of a Fz autonomous clone in which Fz has 0.01% of wild-type interaction with Dsh. (**C**) fz^{R52} (nonautonomous) and fz^{F31} (autonomous) clones with Vang::YFP in nonmutant cells. Vang accumulates at all boundaries of the fz^{F31} but not the fz^{R52} clones (arrowheads). (**D**) Dsh::GFP and Flamingo (Fmi) localization in wild-type, fz^{R52} (null), as well as fz^{F31} and fz^{J22} (autonomous) wings, viewed on the apical surface (top) or in edge cells (bottom three rows). Fmi staining identifies the correct focal plane.

lele, Vang is recruited to the boundary between wild-type and mutant cells, whereas substantially less Vang is recruited to those boundaries in cells adjoining clones of the nonautonomous fz^{R52} allele (Fig. 4C, arrowheads). Thus, $Fz^{autonomous}$ proteins recruit Vang to the opposing cell surface, whereas nonautonomous alleles do not. The second prediction is that autonomous Fz proteins should fail to recruit Dsh. Indeed, we find that both are substantially impaired in Dsh recruitment, though somewhat less impaired than the very strong, nonautonomous fz^{R52} allele (Fig. 4D). Thus, strong *fz* alleles, many of which fail to accumulate Fz protein (*27*), display no or severely impaired interaction with Dsh and Vang, whereas autonomous alleles have impaired interaction with Dsh, but retain substantial ability to recruit Vang to the adjacent membrane. Notably, simulated overexpression of Fz with impaired Dsh interaction also produced the correct polarity disruption in cells proximal to the clones [fig. 9; (*17*)].

The Dsh^1 protein produces nearly autonomous clones, and it carries a mutation in its DEP domain, which is required for membrane localization (*16*, *19*); autonomous *fz* alleles bear point mutations in the first cytoplasmic loop (*27*), suggesting these mutations may affect the same interaction. A low affinity interaction between the Dsh PDZ domain and a sequence in the cytoplasmic tail of Fz has been demonstrated (*31*). Our data suggest that sequences in the Dsh DEP domain, and in the Fz first intracellular loop, are also important for Dsh membrane association. Thus, a regulated, bipartite, high affinity association of Dsh with Fz may be selectively disrupted in $fz^{autonomous}$ alleles.

The ability of our mathematical model to simultaneously reproduce all of the most characteristic PCP phenotypes (table S2) demonstrates the feasibility of the underlying biological model as a PCP signaling mechanism. Further, the mathematical model demonstrates how the overall scheme of the model—a local feedback loop between adjacent cells amplifying an initial asymmetry—can explain the autonomous and nonautonomous behavior of PCP mutant clones. Alternative models invoking diffusible factors have not been supported by the identification of such factors (*12*), and the contact-dependent intercellular signaling model more readily accounts for the slight nonautonomy of *dsh* and $fz^{autonomous}$ clones than do the diffusible factor models.

The ability of the mathematical model to make predictions and provide a detailed picture of PCP signaling is limited by the lack of complete biological understanding. Although the validity of quantitative model predictions is subject to its assumptions and the set of features used in parameter identification (SOM text), the model has allowed us to directly connect a biological model to the complex behaviors it was hypothesized to explain and to explore the implications of variations in the model.

References and Notes

1. P. N. Adler, *Dev. Cell* **2**, 525 (2002).
2. D. R. P. Tree, D. Ma, J. D. Axelrod, *Semin. Cell Dev. Biol.* **13**, 217 (2002).
3. J. Taylor, N. Abramova, J. Charlton, P. N. Adler, *Genetics* **150**, 199 (1998).
4. T. Wolff, G. M. Rubin, *Development* **125**, 1149 (1998).
5. D. Gubb, A. Garcia-Bellido, *J. Embryol. Exp. Morphol.* **68**, 37 (1982).
6. C. R. Vinson, P. N. Adler, *Nature* **329**, 549 (1987).
7. G. Struhl, D. A. Barbash, P. A. Lawrence, *Development* **124**, 2155 (1997).
8. M. Wehrli, A. Tomlinson, *Development* **125**, 1421 (1998).
9. P. A. Lawrence, J. Casal, G. Struhl, *Development* **126**, 2441 (1999).
10. P. N. Adler, J. Taylor, J. Charlton, *Mech. Dev.* **96**, 197 (2000).
11. D. Strutt, R. Johnson, K. Cooper, S. Bray, *Curr. Biol.* **12**, 813 (2002).
12. P. A. Lawrence, J. Casal, G. Struhl, *Development* **129**, 2749 (2002).
13. M. Fanto *et al.*, *Development* **130**, 763 (2003).
14. M. P. Zeidler, N. Perrimon, D. I. Strutt, *Genes Dev.* **13**, 1342 (1999).
15. P. A. Lawrence, J. Casal, G. Struhl, *Development* **131**, 4651 (2004).
16. J. D. Axelrod, *Genes Dev.* **15**, 1182 (2001).
17. D. I. Strutt, *Mol. Cell* **7**, 367 (2001).
18. D. R. P. Tree *et al.*, *Cell* **109**, 371 (2002).
19. J. D. Axelrod, J. R. Miller, J. M. Shulman, R. T. Moon, N. Perrimon, *Genes Dev.* **12**, 2610 (1998).
20. D. Gubb *et al.*, *Genes Dev.* **13**, 2315 (1999).
21. R. Bastock, H. Strutt, D. Strutt, *Development* **130**, 3007 (2003).
22. C. Yang, J. D. Axelrod, M. A. Simon, *Cell* **108**, 675 (2002).
23. D. Ma, C. H. Yang, H. McNeill, M. A. Simon, J. D. Axelrod, *Nature* **421**, 543 (2003).
24. J. Casal, G. Struhl, P. Lawrence, *Curr. Biol.* **12**, 1189 (2002).
25. M. Hannus, F. Feiguin, C. P. Heisenberg, S. Eaton, *Development* **129**, 3493 (2002).
26. H. Strutt, D. Strutt, *Dev. Cell* **3**, 851 (2002).
27. K. H. Jones, J. Liu, P. N. Adler, *Genetics* **142**, 205 (1996).
28. A. M. Turing, *Philos. Trans. R. Soc. London B Biol. Sci.* **237**, 37 (1952).
29. P. N. Adler, personal communication.
30. K. Amonlirdviman, unpublished observations.
31. H. C. Wong *et al.*, *Mol. Cell* **12**, 1251 (2003).

32. This work was supported by the Defense Advanced Research Projects Agency BioInfoMicro (C.J.T.) and BioComp (C.J.T. and J.D.A.) Programs, Stanford's Bio-X IIP (J.D.A. and C.J.T.), NIH R01-GM59823 (J.D.A.), a National Defense Science and Engineering Graduate fellowship (K.A.), a Burt and Deedee McMurtry Stanford Graduate Fellowship (K.A.) and a PHS grant awarded by the National Cancer Institute, DHHS (W.-S.C.). We thank H. McAdams for the initial suggestion of the problem and R. Ghosh for contributions to the mathematical model.

Supporting Online Material

www.sciencemag.org/cgi/content/full/307/5708/423/DC1
Materials and Methods
SOM Text
Figs. S1 to S16
Tables S1 and S2
References and Notes

21 September 2004; accepted 29 November 2004
10.1126/science.1105471

Visfatin: A Protein Secreted by Visceral Fat That Mimics the Effects of Insulin

Atsunori Fukuhara,[1,2*] Morihiro Matsuda,[1*] Masako Nishizawa,[3*] Katsumori Segawa,[1] Masaki Tanaka,[1] Kae Kishimoto,[3] Yasushi Matsuki,[3] Mirei Murakami,[4] Tomoko Ichisaka,[4] Hiroko Murakami,[3] Eijiro Watanabe,[3] Toshiyuki Takagi,[1] Megumi Akiyoshi,[3] Tsuguteru Ohtsubo,[3] Shinji Kihara,[5] Shizuya Yamashita,[5] Makoto Makishima,[1] Tohru Funahashi,[5] Shinya Yamanaka,[4] Ryuji Hiramatsu,[3] Yuji Matsuzawa,[6] Iichiro Shimomura[1,5,7]†

Fat tissue produces a variety of secreted proteins (adipocytokines) with important roles in metabolism. We isolated a newly identified adipocytokine, visfatin, that is highly enriched in the visceral fat of both humans and mice and whose expression level in plasma increases during the development of obesity. Visfatin corresponds to a protein identified previously as pre–B cell colony-enhancing factor (PBEF), a 52-kilodalton cytokine expressed in lymphocytes. Visfatin exerted insulin-mimetic effects in cultured cells and lowered plasma glucose levels in mice. Mice heterozygous for a targeted mutation in the visfatin gene had modestly higher levels of plasma glucose relative to wild-type littermates. Surprisingly, visfatin binds to and activates the insulin receptor. Further study of visfatin's physiological role may lead to new insights into glucose homeostasis and/or new therapies for metabolic disorders such as diabetes.

Recent work in obesity research has revealed that adipose tissue functions as an endocrine organ, producing a variety of secreted factors including leptin (*1*), adiponectin/ACRP30/AdipoQ (*2*–*4*), tumor necrosis factor–α (TNF-α) (*5*), resistin (*6*), and plasminogen